A Raman Confocal Microspectroscopic Study on Azopolymer Holographic Diffraction Gratings: Photo- and Mass Transport-induced Effects on the Molecular Orientation

F. Lagugné Labarthet, T. Buffeteau and C. Sourisseau*

Laboratoire de Physicochimie Moléculaire (UMR 5803 - CNRS), Université Bordeaux I, 33405 Talence, France

SUMMARY: Using the confocal microspectrometric technique we have recorded various resonance enhanced polarized Raman spectra from the surface profile of a permanent holographic diffraction grating prepared by interfering two circularly contra-rotating polarized laser beams on a thin amorphous copolymer film containing azobenzene moities (pDR1M-co-MMA). Different theoretical equations of the Raman scattering intensities, including a treatment taking account for the effect of the high numerical aperture objective, are thus derived. Calculations and simulations of these equations allow for the first time to extract the second $<P_2>$ and fourth $<P_4>$ coefficients of the chromophore orientation function in the various regions and to obtain the corresponding information entropy distribution functions. We then discuss both contributions of the photo- and mass transport- induced effects in the grating formation mechanisms and confirm the existence of a significant dye concentration gradient ($\Delta N/N \approx 5.1 \pm 1.1\%$) in between the top and bottom regions. All the results are consistent with the model of a viscoelastic flow of the polymer involving large pressure gradients and translational diffusion dynamics.

Introduction

Several groups[1, 2] have already found that large surface relief gratings can be directly recorded on Azo-dye-containing polymer thin films using only two interfering polarized laser beams. It has been evidenced that two distinct and competing processes, i.e. the formation of a birefringence grating and a surface relief grating, are taking place. The large surface modulation, as clearly evidenced by Atomic Force Microscopy, has been assigned to a polymer chain migration or photoinduced translational diffusion occurring in the viscoelastic state of the polymer [2,3]. In the present study taking advantage of the spatial resolution of the Raman confocal micro-spectrometry, we have recorded for the first time different resonance enhanced polarized Raman spectra over large area of the grating surface profiles. Using this method, one can obtain at a submicrometer level the chomophore orientation functions, $f(\theta)$, and an estimate of the dye concentration gradients at the top and the bottom regions of the surface relief.

Experimental

Dynamical grating formation experiments were performed on functionalized polymer films (pDR1M-*co*-MMA; 12% DR1M) and Λ=3μm period gratings (θ=5°, λ=514.5nm) were inscribed. The Raman spectra were recorded in the back-scattering geometry on a Labram I

 CCC 1022-1360/98/$ 17.50

(Dilor-France) micro-spectrometer in conjunction with a confocal microscope (100X). In order to avoid any thermal or bleaching effect, a minimum intensity power (~30 μW) of the 632.8 nm incident beam from an He-Ne laser was used even though this laser wavelength is outside the absorption band contour of the chromophore. The configuration set-up of the instrument (see details in ref 4) and of the grating samples are shown in Fig. 1.

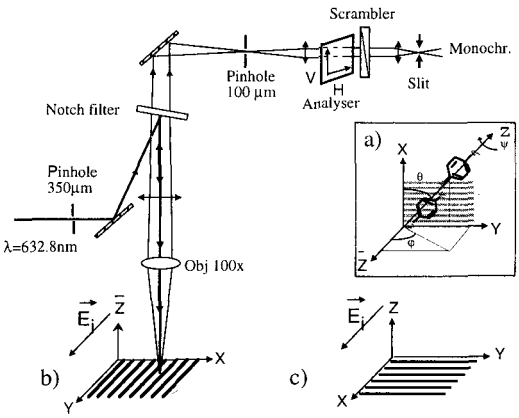

Fig.1: Experimental set-up for the polarized micro-Raman measurements. (a) Axis definition. (b) Measurements of the $z(YY)\bar{z}$, $z(YX)\bar{z}$ spectra in the first configuration. (c) Measurements of the $z(XX)\bar{z}$, $z(XY)\bar{z}$ ones in the second configuration.

Theoretical treatment of the Raman intensities

Because of the cylindrical symmetry of DR1 chromophores and of the effective resonance Raman scattering processes, the following diagonal molecular polarizability tensor and intensity expressions are considered:

[1] $$\overleftrightarrow{\alpha} = \begin{pmatrix} \alpha_1 & 0 & 0 \\ 0 & \alpha_1 & 0 \\ 0 & 0 & \alpha_3 \end{pmatrix}$$

[2] $$I_{IJ}^{0} = C \cdot I_{pump} \cdot \left\langle \alpha_{IJ}^{2} . n_T \right\rangle$$

The average quantity <...> stands for

[3] $$\left\langle \alpha_{IJ}^{2} . n_T \right\rangle = \int_0^{2\pi} d\psi \int_0^{2\pi} d\varphi \int_{-1}^{1} d(\cos\theta) . n_T(\theta) . \left[T(\theta,\varphi,\psi) . \overleftrightarrow{\alpha} . T^t(\theta,\varphi,\psi) \right]^2$$

and is calculated using the normal T and transposed T^t Euler angle matrices; θ is the angle between the main molecular axis and the in-plane X grating axis (Fig. 1a). For a linear polarization state of the incident beam, either parallel (//) (Fig.1b) or perpendicular (⊥) (Fig. 1c) to the grating grooves, the back-scattered intensity expressions for an isotropic sample are:

[4] $$I_{XX}^{\perp,0} \propto \left\langle \alpha_{XX}^{2} . n_T \right\rangle = \frac{N}{15}(8\alpha_1^2 + 3\alpha_3^2 + 4\alpha_1\alpha_3) = I_{YY}^{//,0}$$

[5] $$I_{XY}^{\perp,0} \propto \left\langle \alpha_{XY}^{2} . n_T \right\rangle = \frac{N}{15}(\alpha_1^2 + \alpha_3^2 - 2\alpha_1\alpha_3) = I_{YX}^{//,0}$$

Now, one must consider that the birefringence gratings are formed by two interfering circularly polarized pump beams. As indicated in Scheme 1, the path difference between the two pumps, $\delta = 2\pi X/\Lambda$, gives rise to electric field components proportional to $\cos\theta_{inc}.\cos(\delta/2)$ and $\sin(\delta/2)$ along the X and Y directions, respectively. Then in the Angular Hole Burning[5] process under weak pump intensities, the calculated polarized Raman intensities are found to be modulated by a term proportional to the pump intensity, J, and to $\cos^2(\delta/2)$. After spatial averaging and assuming that the α_3 tensor element is dominant under resonance Raman conditions, one gets:

[6] $$I_{(YY)} = \left(I_{YY}^{//,0} - J.I_{YY}^{//,1}\right) \propto \frac{N}{105}.\alpha_3^2.\left[21 - 15.J + 12.J.\cos^2(\frac{\delta}{2})\right]$$

[7] $$I_{(YX)} = \left(I_{YX}^{//,0} - J.I_{YX}^{//,1}\right) = I_{(XY)} \propto \frac{N}{105}.\alpha_3^2.\left[7 - 3.J + J.\cos^2(\frac{\delta}{2})\right]$$

[8] $$I_{(XX)} = \left(I_{XX}^{\perp,0} - J.I_{XX}^{\perp,1}\right) \propto \frac{N}{105}.\alpha_3^2.\left[21 - 3.J - 6.J.\cos^2(\frac{\delta}{2})\right]$$

Consequently, the above equations [6-8] show that in the first experimental configuration (Fig. 1b) both Raman intensities $I_{(YY)}$ and $I_{(YX)}$ will be maxima for $\delta=0$ (at the tops) and minima for $\delta=\pi$ (at the bottoms of the surface relief) and their Raman images should be in-phase. In contrast, in the second experimental geometry (Fig. 1c), the $I_{(XX)}$ Raman intensities will maximized for $\delta=\pi$ and minimized for $\delta=0$, so that both $I_{(XX)}$ and $I_{(XY)}$ Raman images should be expected out-of-phase. This is a very important result, nicely verified in the experiments (Fig. 2), which will allow us to properly combine all the Raman results in order to obtain the variations of the relative Raman intensitiy ratios,

[9] $$R_1(\delta) = \frac{I_{(YX)}}{I_{(YY)}} \qquad \text{and} \qquad R_2(\delta) = \frac{I_{(XY)}}{I_{(XX)}}$$

and to extract values of the orientation coefficients in the various regions of the grating.

Estimation of the $<P_2>$ and $<P_4>$ coefficients in the chromophore orientation functions

One considers now that all the photo- and transport-induced effects lead to anisotropic samples with localized regions keeping an uniaxial symmetry around the in-plane X axis of the grating (Scheme 1). The angular distributions of the chromophores are thus expressed by developing the function $f(\theta)$ on basis of the first even parity terms in Legendre's polynomials:

$$\left\langle n_T \right\rangle = \frac{N}{4\pi^2}\int_0^{2\pi} d\psi \int_0^{2\pi} d\varphi \int_{-1}^{+1} f(\theta) d(\cos\theta) = N.\int_{-1}^{+1} \sum_{\ell=0,2,4} \left(\frac{2\ell+1}{2}\right).\left\langle P_\ell \right\rangle.P_\ell(\cos\theta).d(\cos\theta)$$

$$\left\langle n_T \right\rangle = N.\int_{-1}^{+1} \left[\frac{1}{2}\left\langle P_0 \right\rangle.P_0(\cos\theta) + \frac{5}{2}\left\langle P_2 \right\rangle.P_2(\cos\theta) + \frac{9}{2}\left\langle P_4 \right\rangle P_4(\cos\theta)\right] d(\cos\theta) \qquad [10]$$

where the coefficients $<P_\ell>$ are the order parameters.

Furthermore, to extract mean values of these order parameters (or of the related $\langle\cos^2\theta\rangle$ and $\langle\cos^4\theta\rangle$ terms) with respect to the effective directions of the incident electric field, an additional rotation ($\alpha = \delta/2$, Scheme 1) around the Z axis has to be considered over the polarizability tensor in order to estimate the orientation function anywhere along the surface relief. The corresponding Raman intensity expressions now depend on the following average quantities:

[11] $$\left\langle \alpha_{IJ}{}^2 \right\rangle = \left\langle \left[R(\alpha).\left[T(\theta,\varphi,\psi).\overleftrightarrow{\alpha}.T^t(\theta,\varphi,\psi) \right].R^t(\alpha) \right]^2 \right\rangle$$

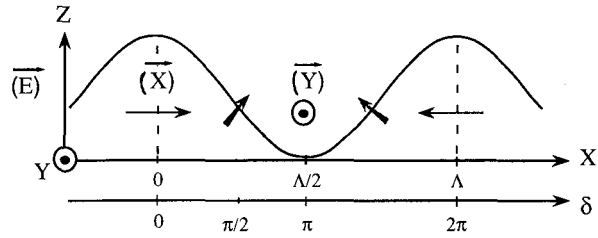

Scheme 1

In addition, in back-scattering Raman microspectrometry it is well known that analyses of polarization measurements must be established using the known optical properties of the wide aperture objective and the refractive index of the sample. According to Turrell'studies[6] and using the above $\left\langle \alpha_{IJ}^2 \right\rangle$ expressions, one must consider the general intensity equations:

[12] $$I_{(YX)} = \left(\left\langle \alpha_{YX}^2 \right\rangle A + \left\langle \alpha_{YZ}^2 \right\rangle B\right)\left(2C_0 + C_2\right) + \left(\left\langle \alpha_{ZX}^2 \right\rangle A + \left\langle \alpha_{ZZ}^2 \right\rangle B\right)\left(4C_1\right) + \left(\left\langle \alpha_{XX}^2 \right\rangle A + \left\langle \alpha_{XZ}^2 \right\rangle B\right)\left(C_2\right)$$

[13] $$I_{(YY)} = \left(\left\langle \alpha_{YY}^2 \right\rangle A + \left\langle \alpha_{YZ}^2 \right\rangle B\right)\left(2C_0 + C_2\right) + \left(\left\langle \alpha_{ZY}^2 \right\rangle A + \left\langle \alpha_{ZZ}^2 \right\rangle B\right)\left(4C_1\right) + \left(\left\langle \alpha_{XY}^2 \right\rangle A + \left\langle \alpha_{XZ}^2 \right\rangle B\right)\left(C_2\right)$$

[14] $$I_{(XY)} = \left(\left\langle \alpha_{XY}^2 \right\rangle A + \left\langle \alpha_{XZ}^2 \right\rangle B\right)\left(2C_0 + C_2\right) + \left(\left\langle \alpha_{ZY}^2 \right\rangle A + \left\langle \alpha_{ZZ}^2 \right\rangle B\right)\left(4C_1\right) + \left(\left\langle \alpha_{YY}^2 \right\rangle A + \left\langle \alpha_{YZ}^2 \right\rangle B\right)\left(C_2\right)$$

[15] $$I_{(XX)} = \left(\left\langle \alpha_{XX}^2 \right\rangle A + \left\langle \alpha_{XZ}^2 \right\rangle B\right)\left(2C_0 + C_2\right) + \left(\left\langle \alpha_{ZX}^2 \right\rangle A + \left\langle \alpha_{ZZ}^2 \right\rangle B\right)\left(4C_1\right) + \left(\left\langle \alpha_{YX}^2 \right\rangle A + \left\langle \alpha_{YZ}^2 \right\rangle B\right)\left(C_2\right)$$

where the quantities A and B are obtained by integration of the squares of the electric vector components over the scattering cone and the coefficients C_0, C_1, C_2 related to the focalisation efficiency are calculated via integration of the incident electric field vector components over the effective irradiated volume[6] . All these parameters are dependent on the angular semi-aperture of the objective (θ_m = 64°.158 for an 100X lens with 0.9 Numerical Aperture) and on the refractive index of the polymer sample (n=1.55), so that we have used the folling values: A= 3.579, B= 0.737, C_0= 6.25, C_1= 0.175 and C_2= 0.00625.

Results and discussion

In general, various set of four distinct polarized Raman spectra (950-1700cm^{-1}) were recorded using both experimental geometries over large grating surface area (16x15μm^2). After intensity integrations, four distinct nicely resolved Raman images were obtained and an illustrative exemple is shown in Fig. 2.

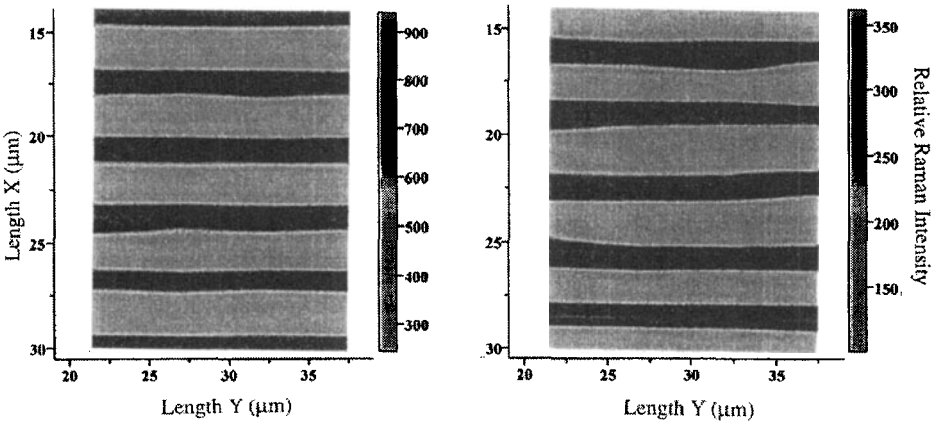

Fig.2: Out of phase $Z(XX)\overline{Z}$ *(left) and* $Z(XY)\overline{Z}$ *(right) Raman images integrated over the 1280-1352cm^{-1} range ($\nu_s NO_2$ mode).*

From the intensities ratios $R_1(\delta)$ and $R_2(\delta)$, $\langle P_2 \rangle$ values were found always negative meanwhile $\langle P_4 \rangle$ ones were alternately negative ($\delta=0$, $2\pi/3$) and positive ($\delta=\pi/3$, π) along the surface grating profile as shown in Table 1.

Tab.1. Average experimental Raman intensity ratios and values of the order parameters and of the Lagrange multipliers in different regions of a 3μm period (Λ) grating.

Λ	δ	$R_1(\delta)$	$R_2(\delta)$	$\langle P_2 \rangle$	$\langle P_4 \rangle$	λ_2	λ_4
0	0	0.390	0.779	-0.124	-0.119	-1.565	-2.054
$\Lambda/6$	$\pi/3$	0.387	0.573	-0.194	+0.124	-0.967	+1.145
$\Lambda/3$	$2\pi/3$	0.400	0.280	-0.138	-0.195	-5.558	-6.434
$\Lambda/2$	π	0.390	0.193	-0.220	+0.187	-1.105	+1.893

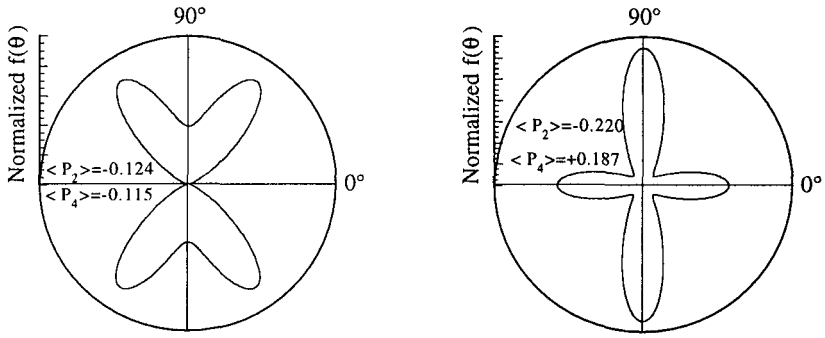

Fig.3: Polar representations of f(θ) in two regions of the grating, δ=0 and δ=π.

We come thus to the important and surprising conclusion that the photo-induced mechanisms in conjunction with the polymer mass transport effects lead to the formation of alternated surface regions of weaker and stronger orientation phenomena. Consequently, the orientational distribution functions in the various grating regions differ significantly and the viscoelastic flow of the polymer chains must be responsible for these effects. Indeed, from the two first even parity order parameters above determined the normalized orientational distribution functions, f(θ) (eq.[16]) , can be estimated by maximizing the information entropy[4,7], and typical f(θ) representations in polar coordinates are shown in Fig. 3.

[16]
$$f(\theta) = \frac{\exp\left[\lambda_2 . P_2(\cos\theta) + \lambda_4 . P_4(\cos\theta)\right]}{\int_{-1}^{+1} \exp\left[\lambda_2 . P_2(\cos\theta) + \lambda_4 . P_4(\cos\theta)\right] . d(\cos\theta)}$$

Therefore, from the experimentally determined $P_2(\cos\theta)$ and $P_4(\cos\theta)$ values, one can estimate the Lagrange multipliers λ_2 and λ_4 by numerically integrations (Table 1).

At δ=0 a broad distribution function is observed with maxima inclined to ±32° with respect to the perpendicular direction while at δ=π the function exhibits a weak maximum at 0° and a stronger one at 90°. These results confirm the important photoinduced orientations in the nearly perpendicular direction of the incoming light and allow us to conclude to the existence of relatively broad distribution functions even in the bottom regions (δ=π). In these regions of greater polymer removal, it is clear that the mass transport phenomena have perturbed to some extent the primary photo-induced orientations.

In addition, as the trans→cis isomerization requires free volume in excess of that available in the starting isotropic film, it is clear that the photochemical reaction produces a laser-induced internal pressure above the yield point of the polymer[4]. Therefore, in complete agreement with Rochon et al.[1] one can imagine a resulting viscoelastic flow of the polymer and the existence

in the various domains of large constraints and stresses which are acting as opposing or restoring forces against the imposed localized orientations. Such a mechanism is reinforced by the fact, as above shown, that the material is removed from the regions of higher perpendicular orientation (at the bottoms) and build up in the regions of weaker orientations (at the tops). Nevertheless, in the intermediate regions the final orientations are found alternately weaker and higher and this could come from competing forces and/or from more or less efficient cooperative orientation effects during the formation of the regularly spaced sinusoidal surface relief grating.

Furthermore, from the knowledge of the various $f(\theta)$ functions and the variations of the relative Raman intensities along the X (or δ) direction, one can get an estimate of the dye concentrations, $N(\delta)$, over the surface relief. From the four sets of recorded polarized Raman spectra, we obtain the average quantity $\langle N(0)/N(\pi)\rangle = 1.11 \pm 0.03$, confirming the existence of a concentration gradient $\Delta N/N = 5.1 \pm 1.1\%$ in between top and bottom regions, as it is summarized in Table 2.

Tab.2. Comparison of experimental and theoretical intensity ratios at the top ($\delta=0$) and bottom ($\delta=\pi$) regions and estimated dye concentration variations and gradients.

$I_{(IJ)}$Spectra	$I(0)/I(\pi)$ exp.	$I(0)/I(\pi)$ theor.	$N(0)/N(\pi)$	$\Delta N/N$ %
YY	780/400=1.950	1.790	1.09	4.31
YX	306/160=1.912	1.770	1.08	3.86
XX	360/850=0.424	0.378	1.12	5.69
XY	290/168=1.726	1.512	1.14	6.63

It is noteworthy that these last results were also confirmed by white lamp irradiation experiments in the visible region using our micro-spectrometer in the transmission or image mode at a fixed wavelength[8]; they are in a good agreement with a translational diffusion model[3], accounting for a concentration modulation in the essential dynamics features of the surface relief grating formation in such amorphous polymer films. Indeed, using in a first approximation the Lorentz-Lorenz approach[9] in order to relate the density contributions to the composition index modulation Δn_C, one can estimate $\Delta n_C = 0.014$; this represents a significant fraction ($\approx 70\%$) of the total index modulation measured by diffraction, $\Delta n_{diff} = 0.020$. In complete agreement with recent optical studies on holographic recording photopolymers[10,11], we thus conclude that a residual density modulation due to pressure gradients created by the viscoelastic flow of the polymer must also contribute to the diffraction.

Conclusion

In this study, by using a modern Raman confocal micro-spectrometer and by analyzing the resonance enhanced polarized Raman spectra recorded on optically inscribed high-efficiency diffraction gratings in azopolymer films, we have obtained for the first time new information about the second $<P_2>$ and fourth $<P_4>$ order parameters of the chromophore orientation functions. In addition, we have demonstrated that the corresponding information entropy distribution functions are different in the various regions of the grating, particularly in the tops and the bottoms of the surface relief. We thus conclude to the existence of large constraints and stresses which probably act as either opposing or restoring forces against the light imposed localized orientations and the translational diffusion mechanisms.

Finally, these measurements provide the first direct evidence of different dye molecular orientations and of a concentration gradient in such diffraction gratings. The high sensitivity and spatial resolution of our Raman confocal micro-spectrometer demonstrates the feasibility of this non-destructive technique in studying photo-induced effects in organic materials.

Acknowledgements

The authors are indebted to the CNRS (Chemistry Department) and to the Région Aquitaine for financial support. They are also thankful to A. Natansohn for providing the functionalized polymer, P. Rochon and M. Pézolet for several fruitful discussions.

References

1) C.J. Barret, A.L. Natansohn, P.L. Rochon, *J.Phys.chem*, **100**, 8836 (1996)

2) X.L. Jiang, Li. Lian, X.L. Jiang, V. Shivshankar, J. Kumar, S.K.Tripathy, *Appl.Phys.lett.* , **68,** 2618 (1996)

3) P. Lefin, C. Fiorini, J.M. Nunzi, *Pure Appl.Opt.* , **7**, 71 (1998)

4) F. Lagugné Labarthet, T. Buffeteau, C. Sourisseau, *J.Phys.Chem.*, **102**, 2654 (1998)

5) Z. Sekkat, M. Dumont, *Synth.Metals* , **54**, 373 (1993)

6) G. Turell, in "Practical Raman Spectroscopies", D.J.Gardiner and P.R. Graves, Eds., Springer Verlag (Berlin), 1989, p.13

7) H. Pottel, W. Herreman, B.W. Van der Meer, M. Ameloot, *Chem.Phys.*, **102**, 37 (1986)

8) F. Lagugné Labarthet, T. Buffeteau, C. Sourisseau, unpublished data.

9) W.J.Tomlinson, E.A. Chandross, *Adv.Photochem.*, **12,** 201 (1980)

10) D.J. Lougnot, P. Jost, L. Lavielle, *Pure Appl. Opt.*, **6**, 225 (1997)

11) C.R. Kagan, T.D. Harris, A.L. Harris, M.L. Schilling,*J.Chem. Phys.*,**108**, 6892 (1998)